Biophysical Journal, Volume *112*

Supplemental Information

Mechanotransduction Dynamics at the Cell-Matrix Interface

Seth H. Weinberg, Devin B. Mair, and Christopher A. Lemmon

Supporting Material for "Mechanotransduction Dynamics at the Cell-Matrix Interface"

S. H. Weinberg, D. B. Mair, C. A. Lemmon

SUPPORTING METHODS

Description of the elastic-stochastic model of FN fibril assembly

In this study, we develop a computational model of fibronectin (FN) fibril assembly and cell-FN fibril-substrate interactions. Our model expands on a prior elastic-stochastic model developed by Chan and Odde (1). In brief, the Chan-Odde model represents a stochastic motor-clutch system, in which traction forces are generated by molecular clutch "engagement" via integrin binding, linking actomyosin forces to the extracellular substrate. Molecular clutches and the substrate are represented by Hookean springs. Most critically distinct from our model described below, in the Chan-Odde model, actomyosin force transmission through engaged elastic molecular clutches occurs directly to the substrate, and the Chan-Odde model does not specifically account for elasticity of and force transmission via ECM proteins at the cell-matrix-substrate interface.

In our model, each FNIII domain is represented by a time-varying Hookean spring (Figure 1A), with spring constant $k_i^j(t)$, where $i \in \{1, \cdots, 30\}$, $j \in \{1, \cdots, N_{FN}(t)\}$ are Type III domain and FN molecule indices, respectively and $N_{FN}(t)$ is the total number of FN molecules in the growing FN fibril and is a function of time t. The FN dimer is comprised of 30 FNIII domains, such that each FN molecule is represented by 30 springs in series. FNI and FNII domains are assumed to be inelastic and non-stretchable. As FN-FN binding occurs during assembly as described below, FN-FN connections are formed between one of the 30 FNIII domains and the N-terminus of a new FN molecule. Thus, the growing fibril is represented by a Hookean spring network with complex architecture defined by the specific FN-FN connections.

Actomyosin forces are transmitted to the assembling FN fibril via integrin connections between the cell surface and the fibril. FNIII-10 bind the $\alpha_5\beta_1$ integrin, which links the FN molecule to a focal adhesion complex (FAC) and transmits actin-dependent force. Extracellular and intracellular signaling within the integrin-FAC-actin system is complex and representing these signaling interactions is beyond the scope of our present model. Following the approach by Chan and Odde (1), we represent the FNIII-10-integrin-FAC-actin connection by a single Hookean spring with spring constant k_c and refer to this connection as a "molecular clutch" (Figure 1A, green springs). Clutch "engagement"/"disengagement" is stochastic and force-dependent. Actomyosin forces, transmitted via engaged clutches, stretch individual FNIII domains (Figure 1B), facilitating the binding of new FN molecules (Figure 1C, red lines). The proba-

bility of FN molecule addition increases with FNIII domain stretch and is also a function of soluble FN concentration. Subsequent integrin binding occurs at the new FN molecule, and the process of FN molecule addition continues until an insoluble, elastic FN fibril is formed (Figure 1D).

Thus, each FN molecule consists of a spring network of 32 springs (30 FNIII domains and 2 clutches). The total number of springs in the FN fibril network at time t is $N^T_{spring}(t) = 32N_{FN}(t) + 1$, where the additional spring represents the substrate (with spring constant k_{sub}), and finally the total number of nodes in the spring network is $N^T_{node}(t) = N^T_{spring}(t) + 1$.

FNIII domain and molecular clutch forces

We define u^j_i as the displacement of the (i,j)-th domain node from its equilibrium position along the z-axis, i.e. displacement in the absence of force. The domain spring constant $k^j_i(t)$ and force $f^j_i(t)$ in the (i,j)-th domain are related to the domain node displacements $u^j_i(t)$ and $u^j_{i+1}(t)$ by Hooke's law,

$$f^j_i = k^j_i(u^j_{i+1} - u^j_i) = k^j_i\epsilon^j_i, \tag{S1}$$

where $\epsilon^j_i = u^j_{i+1} - u^j_i$ is the elongation or stretch of the (i,j)-th FNIII domain. Similarly, the clutch spring constant k_c and force $f^j_{c,m}(t)$ in the (m,j)-th clutch are related by

$$f^j_{c,m} = k_c(u^j_{c,m} - u^j_{10m+1}), \tag{S2}$$

where $m \in \{1,2\}$ is the index of the clutch and $u^j_{c,m}(t)$ is the displacement of the (m,j)-th clutch node from its equilibrium position. The displacement $u^j_{10m+1}(t)$ represents the displacement of the two FNIII-10 domains in the j-th FN dimer, with indices 11 and 21, respectively. The displacement of the substrate spring nodes are given by $u_{sub,0}$ and $u_{sub,1}$, where one end of the spring is "fixed," i.e., $u_{sub,0} = 0$ is an imposed relationship, or boundary condition, and the other substrate spring node is attached to FNIII-1 of the first FN dimer, i.e., $u_{sub,1} = u^1_1$. Thus, the elongation or stretch of the substrate $\epsilon_{sub} = u_{sub,1} - u_{sub,0} = u_{sub,1} = u^1_1$. For ease of notation later, we define $u^1_0 = u_{sub,0} = 0$.

Integrin binding

Integrin binding, i.e., molecular clutch engagement/disengagement, reactions for the (m,j)-th clutch are represented by a first-order reversible reaction,

$$\text{(disengaged) } \mathcal{D} \underset{\bar{\nu}^j_{m,off}}{\overset{\nu_{on}}{\rightleftharpoons}} \mathcal{E} \text{ (engaged)}, \tag{S3}$$

where ν_{on} and $\bar{\nu}^j_{m,off}$ are rates with units of inverse time. Engaged clutches build tension, as the connection via the clutch spring is stretched by actin motion. The

tension in engaged clutches increases the off-rate $\bar{\nu}^j_{m,off}$ exponentially, following a Bell model (2),

$$\bar{\nu}^j_{m,off} = \nu_{off} \exp(f^j_{c,m}/f_b), \tag{S4}$$

where ν_{off} is the disengagement rate in the absence of clutch displacement and f_b is a break force. Thus as $f^j_{c,m}$ increases (Eq. S2), the disengagement rate increases, and the clutch bond becomes more likely to break.

Actomyosin-dependent FN fibril stretch

We assume that actomyosin forces will slow when acting against an elastically loaded substrate according to a linear force-velocity relationship (1),

$$v_{act} = v_u \left(1 - \frac{k_{sub}\epsilon_{sub}}{f_{stall}}\right), \tag{S5}$$

where v_{act} is the actin velocity, v_u is the unloaded actin velocity, ϵ_{sub} is the displacement of the substrate, and $f_{stall} = N_{myo}f_{myo}$ is a stall force that is given by the number of myosin motors N_{myo} and unitary myosin motor force f_{myo}. When substrate force $f_{sub} = k_{sub}\epsilon_{sub}$ is equal to the stall force f_{stall}, the actin filament "stalls," terminating FN assembly.

If we define $\sigma^j_{c,m} \in \{0, 1\}$ as the state of the (m, j)-th molecular clutch, such that $\sigma^j_{c,m} = 0$ or 1 when the clutch is disengaged or engaged, respectively, then the time-dependent dynamics of the clutch displacement $u^j_{c,m}$ is given by

$$\frac{du^j_{c,m}}{dt} = \sigma^j_{c,m} v_{act}. \tag{S6}$$

FNIII domain and molecular clutch node displacement

The temporal dynamics of the displacement of engaged clutches are given by Eq. S6, which in turn transmits actomyosin forces that alter the position of all nodes in the spring network. We assume that FNIII domain node positions are in a rapid equilibrium, such that node positions can be solved by the direct stiffness method, a standard finite element method approach (3). Formally, we solve the linear system given by

$$\mathbf{K}\boldsymbol{u} = \boldsymbol{f}, \tag{S7}$$

where $\mathbf{K}(t)$ is the $N^T_{node} \times N^T_{node}$ global stiffness matrix assembled from the time-dependent spring constants $k^j_i(t)$, $\boldsymbol{u}(t)$ is the $N^T_{node} \times 1$ column vector of displacements

$$\boldsymbol{u} = (u^1_0, u^1_1, \cdots, u^1_{30}, u^1_{c,1}, u^1_{c,2}, u^2_1, \cdots, u^{N_{FN}}_{30}, u^{N_{FN}}_{c,1}, u^{N_{FN}}_{c,2})^T,$$

and $\boldsymbol{f}$ is a $N^T_{node} \times 1$ column vector of external forces.

The engaged clutch displacement(s) and fixed substrate position are imposed as boundary conditions on Eq. S7, which introduces non-zero elements in $\boldsymbol{f}_{red}$, resulting in the reduced linear system,

$$\mathbf{K}_{red}\boldsymbol{u}_{red} = \boldsymbol{f}_{red}. \tag{S8}$$

and the position of the nodes are given by $\boldsymbol{u}_{red} = \mathbf{K}_{red}^{-1}\boldsymbol{f}_{red}$.

Time-varying FNIII domain spring constants

Each FNIII domain is represented by a time-varying Hookean spring. In the absence of actomyosin forces, each FNIII domain spring constant k_i^j is equal to a unique spring constant $k_{i,0}$ (see Table S2), representing the unique mechanical properties of each FNIII domain, while in the presence of large actomyosin forces, domain stiffness values are governed by a worm-like chain (WLC) model, which accounts for the highly nonlinear increase in domain stiffness k_i^j as domain elongation ϵ_i^j increases (4, 5). Recent studies have demonstrated that the WLC model yields similar predictions to molecular dynamics simulations of protein unfolding under high force (6).

The WLC model relates the molecular force F_ω and stretch or elongation ϵ by the following equation:

$$F_\omega(\epsilon) = \left(\frac{k_B T}{\chi_p}\right)\left[\frac{1}{4(1-\epsilon/\chi_d)^2} - \frac{1}{4} + \frac{\epsilon}{\chi_d}\right], \tag{S9}$$

where k_B is Boltmann's constant, T is the absolute temperature, χ_p is the domain persistant length, and χ_d is the domain contour length. To relate this WLC model to the spring network that is the basis of our model, we define the spring constant k_ω relating the force F and displacement ϵ of spring from rest as the derivative of F_ω in Eq. S9, with respective to ϵ,

$$k_\omega(\epsilon) = \frac{dF_\omega}{d\epsilon} = \left(\frac{k_B T}{\chi_d \chi_p}\right)\left[\frac{1}{2(1-\epsilon/\chi_d)^3} + 1\right]. \tag{S10}$$

We model the time-varying domain stiffness $k_i^j(t)$ as a first-order isomerization reaction, such that $k_i^j(t)$ exponentially relax to a domain stretch-dependence steady-state domain stiffness $k_i^\infty(\epsilon_i^j)$, with time constant τ_ω,

$$\frac{dk_i^j}{dt} = \frac{k_i^\infty(\epsilon_i^j) - k_i^j}{\tau_\omega}. \tag{S11}$$

The steady-state domain stiffness k_i^∞ transitions between the ϵ_i^j-dependent regimes for unique stiffnesses and the (identical) WLC-governed stiffnesses, i.e., $k_i^\infty(0) = k_{i,0}$, and for large ϵ_i^j, $k_i^\infty(\epsilon_i^j)$ approaches $k_\omega(\epsilon_i^j)$ (see Figure 3),

$$\hat{k}_i^\infty(\epsilon_i^j) = k_\omega(\epsilon_i^j) + [k_{i,0} - k_\omega(0)]\exp(-\epsilon_i^j/\lambda_\omega), \tag{S12}$$

where λ_ω is a space constant that defines the regime transition. Finally, since $k_\omega(\epsilon) \to \infty$ as $\epsilon \to \chi_d$, for numerical stability, we define a maximum domain stiffness k_{max} and define k_i^∞ as the minimum value of k_{max} and $\hat{k}_i^\infty(\epsilon_i^j)$.

Soluble FN binding and fibril assembly

In our model, FN binding is treated as a two-step process: binding sites are exposed via a stretch-dependent mechanism and soluble FN binds to an exposed binding site. We assume that for the (i,j)-th domain, the probability of FN binding site exposure π_i^j is a function of domain stretch ϵ_i^j and given by a Hill-type equation,

$$\pi_i^j = \frac{(\epsilon_i^j)^\eta}{(\epsilon_i^j)^\eta + \epsilon_t^\eta}, \tag{S13}$$

where ϵ_t is the stretch-dependent threshold, in units of length, and η is a scaling factor that determines the threshold steepness.

Following binding site exposure, an irreversible reaction between soluble FN, $\mathcal{S}$, and the exposed binding site, Δ_i^j, resulting in FN-FN binding, $\mathcal{B}_i^j$, at the (i,j)-th domain:

$$\mathcal{S} + \Delta_i^j \xrightarrow{\nu_{FN}} \mathcal{B}_i^j, \tag{S14}$$

a reaction that occurs with a rate of $\nu_{FN}[\mathcal{S}]$, where $[\mathcal{S}]$ is the concentration of soluble FN in the extracellular space.

FN fibril geometry

The Hookean spring network is 1-dimensional, with actomyosin forces and FNIII domain and clutch displacements occurring along with the z-axis. However, we account for the location of each FN molecule in the (x,y)-plane, assuming that the FN fibril assembles via hexagonal packing with spacing $2r$, where r is the radius of each FN molecule, modeled as a 3-dimensional cylinder. Thus, each FN molecule has a maximum of 6 "neighbors" in the (x,y)-plane. Once the j-th FN molecule has 6 neighbors, either via its own connections or connections of its neighbors, the FN molecule is consider an "interior" FN molecule and can no longer make additional FN-FN connections. Further, we assume that FN-FN bonds do not break once formed.

Importantly, the FNIII-10 integrin binding sites of interior FN molecule are no longer exposed to the cell surface. To account for the inaccessibility of these molecular clutches, we set the clutch engagement rate $\nu_{m,on}^j = 0$ for these FN molecules.

Simulations and analysis

Numerical simulations are performed for 30 hours or until assembly is terminated by "stalled" actomyosin forces (see Eq. S5). For each simulation, we measure the size of the terminal FN fibril (stretched/relaxed length, thickness, number of FN molecules), as well as traction forces and clutch engagement. For the baseline parameter set ($k_{sub} = 1000$ pN/nm), we run 500 simulations, and for all other k_{sub} values, we run 100 simulations.

Numerical simulation implementation

Overview of the hybrid deterministic-stochastic simulation algorithm

Simulation of FN fibril assembly involves time scales ranging over several orders of magnitude: Molecular clutch engagement/disengagement are stochastic events occurring on the order of milliseconds, while FN fibril assembly occurs on the order of hours to days. In order to simulate fibril assembly, we utilize a multiscale hybrid stochastic-deterministic integration scheme that enables the use of a relatively large numerical integration time step, while still appropriately accounting for clutch engagement/disengagement stochastic events.

In general, in order to simulation the stochastic chemical interactions of a system of chemical species interacting via elementary processes (i.e., biochemical reactions), we compute the *propensity function* for each reaction $a_q(\boldsymbol{X}(t))$, which has the property that, to first-order, the probability $p_q(t)$ of the *q-th* reaction taking place in the infinitesimal time interval $[t, t+dt)$ is given by $p_q(t) = a_q(\boldsymbol{X}(t))dt$, where vector $\boldsymbol{X}(t)$ collects the state of all chemical species. For a stochastic simulation with fixed time step to be meaningful, $p_q(t)$ must be less than 1, and further $p_q(t)$ must be small, typically 0.01-0.05, such that the system dynamics do not change significantly within a single time step. This requirement places an strict limitation on the time step dt chosen. For the clutch engagement/disengagement reversible reaction for the (m, j)-*th* clutch (Eq. S3), the individual elementary processes, $\mathcal{D} \rightarrow \mathcal{E}$ and $\mathcal{E} \rightarrow \mathcal{D}$, have propensity functions given by $a_1 = \nu^j_{m,on}(1 - \sigma^j_{c,m})$ and $a_2 = \bar{\nu}^j_{m,off}\sigma^j_{c,m}$, respectively. In order to avoid using a prohibitively small time step, we use the stochastic simulation algorithm, also known as Gillespie's method, which is an exact algorithm without an inherent time step (7).

In brief, Gillespie's method is an iterative stochastic algorithm in which random numbers are drawn in order to determine the time until the next reaction occurs and which reaction occurs at that time. If $a_{sum}(\boldsymbol{X}(t)) = \sum_q a_q(\boldsymbol{X}(t))$, then the time until the next reaction occurring τ is given by

$$a_{sum}(\boldsymbol{X}(t))\tau = \xi, \tag{S15}$$

where ξ is an exponentially distributed random variable (r.v.), which in practice can be determined by drawing an uniformly distributed r.v. U_1 and defining $\xi = -\ln U_1$. If there multiple possible reactions, then the reaction that occurs after time τ, reaction n, is given by the smallest integer n that satisfies

$$\frac{\sum_q^n a_q(\boldsymbol{X}(t))}{a_{sum}(\boldsymbol{X}(t))} < U_2, \tag{S16}$$

where U_2 is a different uniformly distributed r.v.

This method is strictly valid with the constraint that the propensity functions remain constant over the time interval $[t, t+\tau)$. However, from Eqs. S2

and S4, it is clear that $\bar{\nu}^j_{m,off}$ is function of the clutch and domain node displacements and therefore a function of time. In this case, Eq. S15 should be replaced with

$$\int_t^{t+\tau} a_{sum}(\boldsymbol{X}(t'))dt' = \xi, \tag{S17}$$

where τ is time until the next reaction (8). In practice, we utilize a hybrid scheme (9), in which we define a global time step Δt (such that number of total global time steps $N_{global} = T_{total}/\Delta t$ and T_{total} is the total simulation time). During each time step, we treat node displacement values as constant, which simplifies the use of Eq. S17 to determine clutch engagement/disengagement events. At the end of each global time step, we update node displacements using Eqs. S6 and S8, as described below.

Simulations are performed with a global time step $\Delta t = 5$ ms, for a duration of 30 hours ($N_{global} = 2.16 \cdot 10^7$ steps) or until actomyosin forces stall (described below). In the following subsections, we describe the initialization, iteration, and termination of the stochastic simulation of FN assembly.

Initialization

At the initial time point, we assume that one FN molecule is connected to the substrate, and both molecules clutches are disengaged. The initial conditions for the simulation are given as follows:

- Initial domain displacements: $u_{sub} = u^1_1 = u^1_2 = \cdots = u^1_{30} = 0$,
- Initial clutch displacements: $u^1_{c,1} = u^1_{c,2} = 0$,
- Initial clutch state: $\sigma^1_{c,1} = \sigma^1_{c,2} = 0$,
- Initial stiffness vector: $\boldsymbol{k} = (k_{sub}, k^1_1, k^1_2, \cdots, k^1_{30}, k_c, k_c)^T \equiv \boldsymbol{k}_0$,
- Initial total number of FN molecules: $N_{FN} = 1$,
- Initial exponential r.v. and previous value P: $\xi = -\ln(U)$, $P = 0$ (see below), where U is a uniform r.v.
- Initial global time: $t_{global} = 0$,
- Initial set of network connection defining architecture: $S_{\mathcal{A}} = \{\emptyset\}$
- A connection matrix A_{conn}, of size $N^T_{spring} \times 2$, is initialized that defines the spring network architecture. Each row corresponds to one spring in the network and columns indicate the (i, j)-th node indices of the spring

endpoints. Thus, the initial value for A_{conn} is given by

$$A_{conn} = \begin{pmatrix} (0,1) & (1,1) \\ (1,1) & (2,1) \\ \vdots & \vdots \\ (30,1) & (31,1) \\ (10,1) & (c1,1) \\ (20,1) & (c2,1) \end{pmatrix},$$

where $c1$ and $c2$ are the indices of the two molecular clutches. The global stiffness matrix $\mathbf{K}$ is initialized using $\boldsymbol{k}$ and A_{conn}.

Note that we define $S_{\mathcal{A}}(t)$ as the ordered sequence or list of FN-FN connections, where by construction the $q\text{-}th$ element of $S_{\mathcal{A}}$ is the index (i, j) of the FN binding site for FN molecule q, at time t. For example, if at some time point t,

$$S_{\mathcal{A}}(t) = \langle \emptyset, (2,1), (4,1), (1,2) \rangle,$$

then, the second FN molecule (in order of assembly), is bound to FNIII-2 (domain 2) of the first FN molecule, which is bound to the substrate. The third FN molecule is connected to FNIII-4 of the first FN molecule, and the fourth FN molecule is connected to FNIII-1 of the second FN molecule. The first FN molecule does not have a FN-FN connection (being connected to the substrate), and by convention we define this connection as the empty set $\emptyset$. Thus, $S_{\mathcal{A}}(t)$ fully defines the architecture of the spring network. Note that the total number of FN molecule in the FN fibril at time t, $N_{FN}(t) = n(S_{\mathcal{A}}(t))$, the number of elements in $S_{\mathcal{A}}(t)$.

Iteration

The following calculations are performed for N_{global} steps and simulation state variables are output at the desired time points:

1. FNIII domain node displacement: After applying the appropriate boundary conditions, the reduced linear system vectors ($\mathbf{K}_{red}$ and $\boldsymbol{f}_{red}$) are determined from the full system ($\mathbf{K}$ and $\boldsymbol{f}$), and the reduced system is solved numerically (Eq. S8):

$$\boldsymbol{u}_{red} = \mathbf{K}_{red}^{-1} \boldsymbol{f}_{red}. \tag{S18}$$

   Domain node displacements u_i^j are updated accordingly from the values in $\boldsymbol{u}_{red}$.

2. Molecular clutch engagement/disengagement: Clutch engagement/disengagement is represented by a reversible first-order reaction (Eq. S3). Each FN molecule has two possible clutch binding sites, at domains 11 and 21, and therefore, there are $2N_{FN}$ clutches in the growing fibril. As discussed

above, we use a modified version of Gillespie's method to simulation clutch engagement/disengagement events:

At the beginning of each global time step, we define a local time $t_{local} = 0$ and perform the following:

- Define the propensity functions for all (m, j)-*th* clutch (dis)engagement events, for $m \in \{1, 2\}$ and $j \in \{1, 2, \cdots, N_{FN}\}$:
  - For engagement events $\mathcal{D} \to \mathcal{E}$: $a_q = \nu^j_{m,on}(1 - \sigma^j_{c,m})$, for $q = 2(j-1) + m$.
  - For disengagement events $\mathcal{E} \to \mathcal{D}$: $a_q = \bar{\nu}^j_{m,off}\sigma^j_{c,m}$, for $q = 2(j-1) + m + 2N_{FN}$, where $\bar{\nu}^j_{m,off}$ is given by Eq. S4.
- Define $a_{sum} = \sum_q a_q$.
  While $t_{local} < \Delta t$
  - *If* $(\xi - P) \leq a_{sum}\Delta t$ (reaction occurs within global time step)
    - The time to next reaction $\tau \leftarrow \xi / a_{sum}$ (Eq. S15).
    - Previous value reset to zero: $P \leftarrow 0$.
    - The index of reaction n that occurs is given by the smallest integer n that satisfies $\sum_q^n a_q < U \cdot a_{sum}$ (Eq. S16), where U is a uniformly distributed r.v.
      - *If* $n \leq 2N_{FN}$ (engagement event occurs): $\sigma^j_{c,m} \leftarrow 1$, where $j = \lceil n/2 \rceil$ and $m = n - 2(j-1)$.
      - *Else if* $n > 2N_{FN}$ (disengagement event occurs): $\sigma^j_{c,m} \leftarrow 0$, where $j = \lceil (n-2N_{FN})/2 \rceil$ and $m = n - 2(j-1) - 2N_{FN}$.
    - *If* $t_{local} + \tau \leq \Delta t$ (local time remains within the global time step)
      - Draw new exponential r.v.: $\xi \leftarrow -\ln(U)$
      - Update local time: $t_{local} \leftarrow t_{local} + \tau$
    - *Else if* $t_{local} + \tau > \Delta t$ (local time exceeds global time step)
      - Draw new exponential r.v.: $\xi \leftarrow -\ln(U) - a_{sum}(\Delta t - t_{local})$
      - Update local time to break loop: $t_{local} \leftarrow \Delta t$
  - *Else if* $(\xi - P) > a_{sum}\Delta t$ (no reaction occurs in global time step)
    - Update previous value: $P \leftarrow P + a_{sum}\Delta t$
    - Update local time to exit *while* loop: $t_{local} \leftarrow \Delta t$

3. Clutch node displacement: Engaged clutch node displacements are updated by numerical integration of Eq. S6 using the forward Euler method:

$$u^j_{c,m} \leftarrow u^j_{c,m} + v_{act}\Delta t, \text{ for all } (m, j) \in S_{\mathcal{E}}, \tag{S19}$$

where actin velocity v_{act} is given by Eq. S5, and $S_{\mathcal{E}}$ is the set of the indices of the engaged clutches, $S_{\mathcal{E}} = \{(m, j) \mid \sigma^j_{c,m} = 1\}$. Note that the

first-order Euler integration method is exact, since v_{act} is constant over each global time step.

By definition, the force in a disengaged clutch $f^j_{c,m}$ is equal to zero. Therefore, the displacement of the disengaged clutch node is given by (Eq. S2)

$$u^j_{c,m} \leftarrow u^j_{10m+1}, \text{ for all } (m,j) \in S \backslash S_{\mathcal{E}}, \tag{S20}$$

where S is the set of all appropriate values of (m,j) and $S \backslash S_{\mathcal{E}} = \{(m,j) \mid \sigma^j_{c,m} = 0\}$ is the set of all disengaged clutches.

4. Time-varying domain stiffnesses: Domain stiffnesses k^j_i are updated by numerical integration of Eq. S11 using the fourth-order Runge Kutta method (RK4):

$$k^j_i \leftarrow k^j_i + \frac{\Delta t}{6}\left(\theta_1 + 2\theta_2 + 2\theta_3 + \theta_4\right), \tag{S21}$$

where $\theta_1 = \mathcal{F}_\Omega(k^j_i, \epsilon^j_i)$, $\theta_2 = \mathcal{F}_\Omega(k^j_i + \frac{1}{2}\theta_1, \epsilon^j_i)$, $\theta_3 = \mathcal{F}_\Omega(k^j_i + \frac{1}{2}\theta_2, \epsilon^j_i)$, $\theta_4 = \mathcal{F}_\Omega(k^j_i + \theta_3, \epsilon^j_i)$, and $\mathcal{F}_\Omega(k^j_i, \epsilon^j_i) = (k^\infty_i(\epsilon^j_i) - k^j_i)/\tau_\omega$. The appropriate values in stiffness vector $\boldsymbol{k}$ are updated.

5. FN-FN binding: We define $\phi^j_i \in \{0,1\}$ as the state of (i,j)-*th* domain, such that $\phi^j_i = 0$ (1) when the domain is not bound (is bound) to a FN molecule. We further define the "neighbor" function $\mathcal{F}_n(j) : j \to \mathcal{N}$, where $\mathcal{N} \in \{1, 2, \cdots, 6\}$ is the number of neighbors for the j-*th* FN molecule.

   - For every FNIII domain, a uniformly distributed r.v. U^j_i is drawn.

   - *If* $\phi^j_i = 0$ (domain is unbound) AND $U^j_i < \pi^j_i$ (binding site is exposed, Eq. S13) AND $\mathcal{F}_n(j) < 6$ (a new FN molecule can bind)
     - Draw a new uniformly distributed r.v. U
     - *If* $U < \nu_{FN}[\mathcal{S}]\Delta t$ (Eq. S14, new FN-FN connection is formed): A connection between the (i,j)-*th* domain and a new FN molecule is added to the growing fibril. Initialize and update the following:
       * Domain state is occupied: $\phi^j_i = 1$,
       * Increase total number of FN molecules: $N_{FN} \leftarrow N_{FN} + 1$,
       * Initialize clutch states: $\sigma^{N_{FN}}_{c,1} = \sigma^{N_{FN}}_{c,2} = 0$,
       * Update stiffness vector: $\boldsymbol{k} \leftarrow (\boldsymbol{k}^T, \boldsymbol{k}_0)^T$
       * Update architecture ordered set: $S_{\mathcal{A}} \leftarrow \langle S_{\mathcal{A}}, (i,j)\rangle$

* Update connection matrix: $A_{conn} \leftarrow \begin{pmatrix} A_{conn} & \\ (1, N_{FN}) & (2, N_{FN}) \\ \vdots & \vdots \\ (30, N_{FN}) & (31, N_{FN}) \\ (10, N_{FN}) & (c1, N_{FN}) \\ (20, N_{FN}) & (c2, N_{FN}) \end{pmatrix}$
  By construction, the index of the first domain of the new FN dimer $(1, N_{FN})$ is equal to the index of the FN-FN connection (i, j).
* *If* FN dimer j has become an interior dimer as discussed above, i.e., $\mathcal{F}_n(j) = 6$: set clutch engagement rates to zero as described above.
* Global stiffness matrix: The global stiffness matrix $\mathbf{K}$ is updated using current values of $\boldsymbol{k}$ and A_{conn}.

6. Global time: The global time step is updated:

$$t_{global} \leftarrow t_{global} + \Delta t. \tag{S22}$$

Termination

- End simulation *if* $t_{global} = T_{total}$ *OR* $v_{act} < 0.005 v_u$ (Actomyosin forces "stall").

Model parameters

Values and the sources for the model parameters are given in the following two tables. Molecular clutch, substrate, and actin parameters are given in Table S1. Most model parameters were based on values given in Chan and Odde (1).

In Table S2, parameter values for the FN Type III domain stiffness values and other FN fibril parameters are given. Several parameters were estimated based on reasonable approximations and estimations from the literature: In order to estimate the resting stiffness values of the FN Type III domains, we first assumed that the resting stiffness values for all FNIII domains were less than the molecular clutch stiffness k_c of 5 pN/nm (from Chan and Odde (1)), such that FN binding events could occur before clutch disengagement events became highly probable. We then estimated the relative mechanical stiffness from recent atomic force microscopy (10), buried cysteine assays (11), and protein denaturation assays (personal communication with Tomoo Ohashi and Harold Erickson).

The domain stiffness relaxation time constant τ_ω was estimated to approximately match the relaxation of the length measurement to its steady-state value and to match the approximate duration for fibril assembly. The domain stiffness space constant λ_ω was estimated such that the elongation-dependent stiffness values were distinct at the domain binding site exposure threshold ϵ_t and comparable for elongations approximately twice ϵ_t (see Figure 3).

To estimate the soluble FN binding rate, ν_{FN}, we assumed that soluble FN binding to an exposed FN binding site is diffusion-limited (i.e., the elementary binding reaction is rapid), then $\nu_{FN} \approx 4\pi r_{FN} D_{FN} N_A$, where $r_{FN} = 9$ nm is the soluble FN fibril radius (12), D_{FN} is the FN diffusion coefficient, and N_A is Avogadro's constant. Based on diffusion rates for plasma FN ($D_{FN} = 2.5 \cdot 10^{-7}$ cm^2 s^{-1}, (12)) and membrane-bound FN ($D_{FN} = 0.7 \cdot 10^{-12}$ cm^2 s^{-1}, (13)) as upper and lower limits, respectively, such that ν_{FN} may range over $4.7 \cdot 10^{-6} - 1.7$ nM^{-1} s^{-1}, we choose an intermediate value of 0.001, assuming that soluble FN diffusion is partially restricted due to the close proximity of the assembling fibril. The domain binding site exposure scaling factor η was chosen to be 6, based on the Hill coefficient for cooperative binding assuming 6 possible binding sites for a hexagonal packing structure for the assembling fibril.

SUPPORTING RESULTS

Number of fibronectin molecules predicts fibril morphometrical and mechanical properties in a substrate-dependent manner

In this section, we more closely investigate the relationship between focal adhesion length and fibril morphometrical and mechanical properties and the substrate stiffness. In Fig. S1, we plot the focal adhesion length and the fibril properties as a function of the number of FN molecules, for different values of substrate stiffness k_{sub}. We compute these measures by averaging the given fibril properties over all time points for which the fibril is composed of the specified number of FN molecules (with windows of 10 FN molecules). Interestingly, we observe that the relationship between some properties and the number of FN molecules depends on substrate stiffness, while other properties do not depend on substrate stiffness.

As expected, stretched and relaxed length and focal adhesion length all increased as the number of FN molecules increases. In general, for a fibril comprised of a given number of FN molecules, the stretched length increases as k_{sub} increases, more so for larger FN molecule values (Fig. S1A). In Fig. 7E, we show that the average stretched fibril length increases as a function of a substrate stiffness k_{sub}. By examining the same relationships for the relaxed length and FN extensibility (stretched/relaxed ratio), we can determine to what extent fibril architecture versus fibril elasticity dictate the stretched fibril length for different substrate stiffness. We find that on soft substrates (k_{sub} = 0.1 pN/nm; dark blue), the relaxed length is shorter, for a given number of FN molecules, compared with larger values of k_{sub}, which suggests that the fibril architecture, and not the stretch of individual Type III domains, is playing a larger role in governing stretched fibril length. In contrast, on more rigid substrates, the relationship between relaxed length and the number of FN molecules does not depend on substrate stiffness, meaning that for a given number of FN molecules, fibril architectures are comparable, regardless of substrate stiffness. However, we find that FN extensibility, in general, increases as a function of substrate stiffness, for a given number of FN molecules (Fig. S1C), which, in conjunction with comparable fibril architectures, demonstrates that individual Type III domains are more stretched as substrate stiffness increases. These predictions are also consistent with the overall increase in FN extensibility as a function of substrate stiffness, observed in Fig. 7G.

A thorough analysis of the model predictions can explain the U-shaped dependence of focal adhesion stress, as a function of substrate stiffness, shown in Fig. 6A. For all substrate stiffnesses, the fraction of attached molecular clutches increases as the number of FN molecules increases (Fig. S1D). However, this fraction is larger on soft substrates, in particular for FN molecule values between 0 and approximately 300 molecules. Interestingly, this does not lead to larger substrate forces. Substrate force increases as the number of FN molecules increases; however this relationship is independent of k_{sub} (Fig. S1E).

Significantly, this suggests that on soft substrates, a fibril comprised of a given number of FN molecules on average has more integrin bound connections, compared with more rigid substrates, but still only generates the same substrate force. Following Eq. 5, actin velocity decreases as the number of FN molecules increases, and is similarly independent of k_{sub} (Fig. S1F). As a consequence, focal adhesion length is smaller on softer substrates, compared to more rigid substrates (Fig. S1G). Thus, smaller focal adhesion length in the presence of comparable substrate forces results in a larger focal adhesion stress on soft substrates. On intermediate substrate stiffnesses (k_{sub} = 10 pN/nm; cyan), focal adhesion length is consistently larger for large numbers of FN molecules, reducing the focal adhesion stress, while on more rigid substrates (k_{sub} = 100 and 1000 pN/nm; yellow, orange), focal adhesion length is moderately smaller, such that focal adhesion stress is increased, producing the U-shaped dependence observed for focal adhesion stress as a function of substrate stiffness.

Further analysis can also explain the seemingly contradictory observation that terminal FN fibrils are, on average, longer but comprised of fewer FN molecules, as observed in Fig. 7E and H, on more rigid substrates. First, we note that the probability of fibril assembly termination, shown as a function of the number of FN molecules, does show a dependence on substrate stiffness (Fig. S1H). This probability increases as a function of FN molecule count, for all substrate stiffness, as expected. For fibrils with a small number of FN molecules (less than 300), the probability of assembly termination is U-shaped as a function of substrate stiffness, that is, fibril assembly is more likely to terminate on either a very soft or very rigid substrate, but less likely to terminate on an intermediate substrate stiffness. However, for a fibril comprised of larger number of FN molecules, this trend shifts, such that the probability of assembly termination decreases as k_{sub} decreases. Collectively, these relationships result in the generally negative correlation between substrate stiffness and the number of FN molecules at assembly termination, observed in Fig. 7H. However, the increase in FN extensibility and elasticity of individual Type III domains on more rigid substrates more than compensates for the fewer number of FN molecules, such that the average stretched length increases as a function of substrate stiffness (Fig. 7E).

Mechanotransduction model predictions of unloaded actin velocity dependence

The above analysis demonstrated that the substrate stiffness provides critical feedback during the fibril assembly process that alters FN extensibility, integrin binding, focal adhesion length, and termination of the assembly process itself. In addition to altering the distribution of cell-generated forces, the substrate stiffness provides this feedback through regulation of the actin velocity, which in turn governs the stretching of the fibril. We next investigated the dependence of the unloaded actin velocity v_u on our model, to demonstrate the dependence

of the velocity on fibril properties. Physiologically, actin velocity can range several orders of magnitude, depending on cell type and myosin phosphorylation, with values ranging from 8 to 4600 nm/s in dephosphorylated myosins from platelet cells to fast skeletal muscle myosins, respectively (14). We first investigated our model on a rigid substrate (k_{sub} = 1000 pN/nm). For slow v_u = 10 nm/s, substrate force f_{sub} of the assembled fibrils remains essentially constant, with small fluctuations due to the breaking and creation of integrin bounds (Fig. S2A, black). In contrast, for fast $v_u = 10^4$ nm/s, f_{sub} remains near zero, with frequent large fluctuations due to integrin rupture events (Fig. S2A, green). An intermediate v_u = 300 nm/s produces an intermediate response, with sustained large substrate forces but significant fluctuations due to integrin binding breakage (Fig. S2A, red, c.f. Fig. 7B in the main text). Thus, our model predicts that, on average, substrate forces decrease as the unloaded actin velocity increases (Fig. S2B), and this result does not depend on the substrate stiffness. Similarly, the average fraction of attached molecular clutches also decreases as the unloaded actin velocity increases, independent of substrate stiffness (Fig. S2C). Critically, we find that a fast actin velocity produces dynamics similar to the frictional slippage regime observed in the Chan-Odde model (Fig. 7A), such that frequent integrin rupture events prevent sustained substrate forces necessary for FN-FN binding events. However, in contrast with the Chan-Odde model, this regime does not depend on substrate rigidity, but rather the cell-state dependent property of actin velocity. These findings confirm experimental evidence that either myosin inhibitors or myosin *activators* impair FN fibril assembly (15).

As a consequence, the fibril assembly processes is increasingly truncated as the unloaded actin velocity increases (Fig. S2D-G), such that stretched length, relaxed length, and the number of FN molecules all decrease as a function of v_u. Further, FN extensibility is also decreased, consistent with reduced extensibility in fibrils of fewer FN molecules in Fig. S1C. The prediction that substrate forces are reduced as actin velocity increases seems surprising, when also considering that larger actin velocities are associated with myosins from cells that generate considerable forces, e.g., fast skeletal muscle. However, it is important to note that the model prediction of reduced substrate force is primarily a consequence of greatly reduced fibril assembly, due to frictional slippage dynamics, independent of substrate stiffness. This has been experimentally confirmed through studies that show that large forces on stiff surfaces require FN assembly, and that inhibition of FN assembly impairs force generation (16). Thus, the model predicts that cells with large actin velocity are not ideal to assemble FN fibrils, but further work is needed to predict how actin velocity and substrate stiffness influence substrate forces for fully assembled FN fibrils. This is of great interest and is an area of ongoing investigation.

SUPPORTING FIGURES

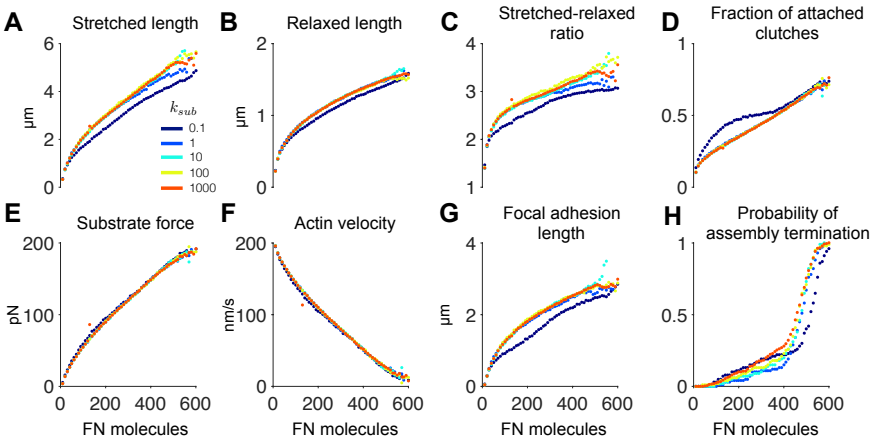

Figure S1: Number of fibronectin molecules predicts fibril morphometrical and mechanical properties in a substrate-dependent manner. (A) Stretched length, (B) relaxed length, (C) fibril extensibility (stretched-relaxed FN length ratio), (D) the fraction of attached molecular clutches, (E) substrate force, (F) actin velocity, (G) focal adhesion length, and (H) the probability of fibril assembly termination are shown as a function of the number of fibronectin (FN) molecules, for different values of substrate stiffness k_{sub}. In panels A-G, each data point is calculated by averaging the given fibril properties over all time points for fibrils composed of the specified number of FN molecules (with windows of 10 FN molecules).

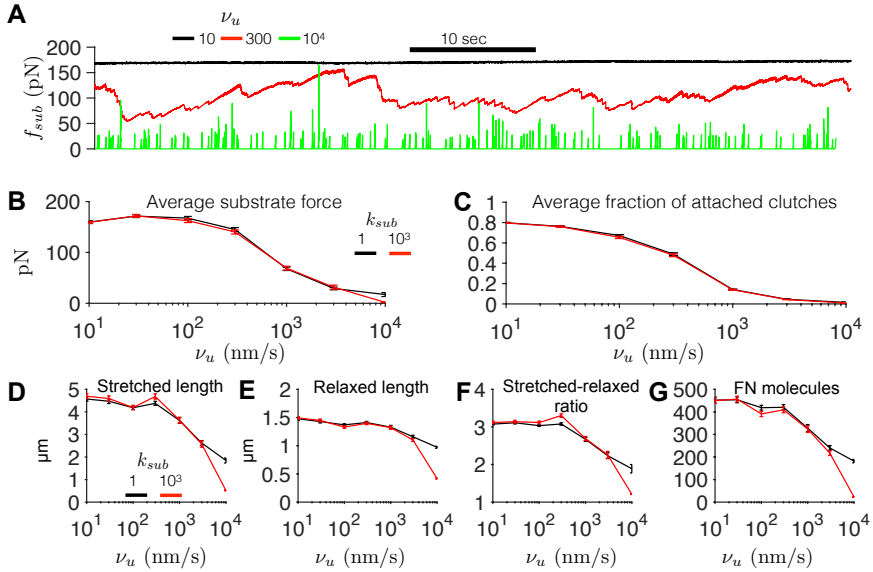

Figure S2: Mechanotransduction model predictions of unloaded actin velocity dependence. (A) Substrate force f_{sub} as a function of time for different unloaded actin velocity values ν_u. Model mean ± standard error, for (B) substrate force and (C) fraction of attached molecular clutches are shown as a function of ν_u for different substrate stiffness values k_{sub}. Mean ± standard error, for (D) stretched length, (E) relaxed length, (F) stretched-relaxed length ratio, and (G) number of FN molecules are shown as a function of ν_u for different substrate stiffness values k_{sub}. In A, $k_{sub} = 1000$ pN/nm. In B-G, model averages are computed by time-averaging over the minute preceding FN assembly termination, and then averaged over 100 simulations.

SUPPORTING TABLES

Table S1: *Molecular clutch, substrate, and actin parameters.*

Parameter	Definition	Units	Value
ν_{on}	Clutch engagement rate	s^{-1}	0.1 (1)
ν_{off}	Unstretched clutch disengagement rate	s^{-1}	0.01 (17)
k_c	Clutch spring constant	pN/nm	5 (1, 18)
f_b	Clutch break force	pN	2 (1, 19)
k_{sub}	Substrate spring constant	pN/nm	0.1-1000
v_u	Unloaded actin velocity	nm/s	200 (14, 20)
f_{stall}	Actin stall force	pN	$N_{myo}f_{myo}$
N_{myo}	Number of myosin motors	-	100 (1)
f_{myo}	Unitary myosin motor force	pN	2 (1, 21)

Table S2: *FNIII domain and fibril parameters.*

Parameter	Definition	Units	Value
$k_{1,0} = k_{30,0}$	FNIII-1 resting stiffness	pN/nm	0.4*
$k_{2,0} = k_{29,0}$	FNIII-2 resting stiffness	pN/nm	0.8*
$k_{3,0} = k_{28,0}$	FNIII-3 resting stiffness	pN/nm	0.3*
$k_{4,0} = k_{27,0}$	FNIII-4 resting stiffness	pN/nm	0.9*
$k_{5,0} = k_{26,0}$	FNIII-5 resting stiffness	pN/nm	1.0*
$k_{6,0} = k_{25,0}$	FNIII-6 resting stiffness	pN/nm	0.6*
$k_{7,0} = k_{24,0}$	FNIII-7 resting stiffness	pN/nm	0.9*
$k_{8,0} = k_{23,0}$	FNIII-8 resting stiffness	pN/nm	0.8*
$k_{9,0} = k_{22,0}$	FNIII-9 resting stiffness	pN/nm	0.7*
$k_{10,0} = k_{21,0}$	FNIII-10 resting stiffness	pN/nm	0.5*
$k_{11,0} = k_{20,0}$	FNIII-11 resting stiffness	pN/nm	0.3*
$k_{12,0} = k_{19,0}$	FNIII-12 resting stiffness	pN/nm	0.6*
$k_{13,0} = k_{18,0}$	FNIII-13 resting stiffness	pN/nm	0.5*
$k_{14,0} = k_{17,0}$	FNIII-14 resting stiffness	pN/nm	0.8*
$k_{15,0} = k_{16,0}$	FNIII-15 resting stiffness	pN/nm	0.7*
k_{max}	Maximum domain stiffness	pN/nm	10^6 (for numerical stability)
τ_ω	Domain stiffness relaxation time constant	s	0.01*
λ_ω	Domain stiffness space constant	nm	1*
χ_d	Domain contour length	nm	30.6 (5)
χ_p	Domain persistence length	nm	0.5 (5)
r	FNIII molecule radius	nm	1 (22)
ϵ_t	Domain binding site exposure threshold	nm	1.5 (23)
η	Domain binding site exposure scaling factor	-	6*
ν_{FN}	Soluble FN binding rate	$\text{nM}^{-1}\ \text{s}^{-1}$	0.001*
$[\mathcal{S}]$	Extracellular soluble FN concentration	nM	20 (24)

* indicates that the parameter value was estimated. See Supporting Methods for details.

SUPPORTING MOVIES

Movie S1: Simulation of fibronectin fibril assembly, shown in Fig. 2 and 4. (Top) The Hookean spring network and position along the z-axis is shown as a function of time. Elastic fibronectin (FN) type III domains (black), FN-FN binding (red), inelastic FN type I and II domains (blue), and integrin binding (green) are shown. (Bottom, left) The FN fibril cross-section in the x-y plane is shown, with FN-FN connections (red). (Bottom, right) The three-dimensional FN fibril architecture is shown. The first hour is shown with 1 minute time increments, and the subsequent 16 hours are shown in 15 minute time increments.

SUPPORTING REFERENCES

[1] Chan, C. E., and D. J. Odde, 2008. Traction Dynamics of Filopodia on Compliant Substrates 322:1687–1691.

[2] Bell, G. I., 1978. Models for the specific adhesion of cells to cells. *Science* 200:618–627.

[3] Ferreira, A. J. M., 2008. MATLAB Codes for Finite Element Analysis, volume 157 of *Solids and Structures*. Springer Science & Business Media, Dordrecht.

[4] Bustamante, C., J. Marko, E. Siggia, and S. Smith, 1994. Entropic elasticity of lambda-phage DNA. *Science* 265:1599–600.

[5] Marko, J. F., and E. D. Siggia, 1995. Stretching DNA. *Macromolecules* 28:8759–8770.

[6] Stirnemann, G., D. Giganti, J. M. Fernandez, and B. Berne, 2013. Elasticity, structure, and relaxation of extended proteins under force. *Proc. Natl. Acad. Sci. U.S.A.* 110:3847–52.

[7] Gillespie, D. T., 1977. Exact stochastic simulation of coupled chemical reactions. *Journal Phys Chem* 81:2340–2361.

[8] Alfonsi, A., E. Cancès, G. Turinici, B. Di Ventura, and W. Huisinga, 2005. Adaptive simulation of hybrid stochastic and deterministic models for biochemical systems. *ESAIM* 14:1–13.

[9] Nivala, M., E. de Lange, R. Rovetti, and Z. Qu, 2012. Computational modeling and numerical methods for spatiotemporal calcium cycling in ventricular myocytes. *Front Physiol* 3:114.

[10] Oberhauser, A. F., B. Carmelu, C. Mariano, and J. M. Fernandez, 2002. The Mechanical Hierarchies of Fibronectin Observed with Single-molecule AFM 319:433–447.

[11] Lemmon, C. A., T. Ohashi, and H. P. Erickson, 2011. Probing the Folded State of Fibronectin Type III Domains in Stretched Fibrils by Measuring Buried Cysteine Accessibility 286:26375–26382.

[12] Mcdonagh, J., 1985. Plasma Fibronectin. Structure and Functions. CRC Press.

[13] Berg, J. M., J. L. Tymoczko, and L. Stryer, 2002. Biochemistry. W. H. Freeman.

[14] Cuda, G., E. Pate, R. Cooke, and J. R. Sellers, 1997. In vitro actin filament sliding velocities produced by mixtures of different types of myosin 72:1767–1779.

[15] Lemmon, C. A., C. S. Chen, and L. H. Romer, 2008. Cell Traction Forces Direct Fibronectin Matrix Assembly 96.

[16] Scott, L. E., D. B. Mair, J. D. Narang, K. Feleke, and C. A. Lemmon, 2015. Fibronectin fibrillogenesis facilitates mechano-dependent cell spreading, force generation, and nuclear size in human embryonic fibroblasts. *Integr Biol (Camb)* 7:1454–65.

[17] Lele, T. P., C. K. Thodeti, J. Pendse, and D. E. Ingber, 2008. Investigating complexity of protein–protein interactions in focal adhesions. *Biochemical and Biophysical Research Communications* 369:929–934.

[18] Fisher, T. E., A. F. Oberhauser, M. Carrion-Vazquez, P. E. Marszalek, and J. M. Fernandez, 1999. The study of protein mechanics with the atomic force microscope. *Trends Biochem. Sci.* 24:379–384.

[19] Jiang, G., G. Giannone, D. R. Critchley, E. Fukumoto, and M. P. Sheetz, 2003. Two-piconewton slip bond between fibronectin and the cytoskeleton depends on talin. *Nature* 424:334–337.

[20] Umemoto, S., A. R. Bengur, and J. R. Sellers, 1989. Effect of multiple phosphorylations of smooth muscle and cytoplasmic myosins on movement in an in vitro motility assay. *Journal of Biological Chemistry* 264:1431–1436.

[21] Molloy, J. E., J. E. Burns, J. Kendrick-Jones, R. T. Tregear, and D. C. White, 1995. Movement and force produced by a single myosin head. *Nature* 378:209–212.

[22] Leahy, D., I. Aukhil, and H. Erickson, 1996. 2.0 A crystal structure of a four-domain segment of human fibronectin encompassing the RGD loop and synergy region. *Cell* 84:155–64.

[23] Gao, M., D. Craig, V. Vogel, and K. Schulten, 2002. Identifying Unfolding Intermediates of FN-III10 by Steered Molecular Dynamics. *Journal of Molecular Biology* 323:939–950.

[24] Ylätupa, S., C. Haglund, P. Mertaniemi, E. Vahtera, and P. Partanen, 1995. Cellular fibronectin in serum and plasma: a potential new tumour marker? 71:578–82.